Dynamics of kink, antikink, bright, generalized Jacobi elliptic function solutions of matter-wave condensates with time-dependent two- and three-body interactions

D. Belobo Belobo,[1,2,*] G. H. Ben-Bolie,[1,2] and T. C. Kofane[2,3,4]

[1]*Laboratory of Atom and Radiation, Department of Physics, Faculty of Science, University of Yaounde I, P.O. Box 812, Yaounde, Cameroon*

[2]*Centre d'Excellence en Technologies de l'Information et de la Communication (CETIC), University of Yaounde I, Yaounde, Cameroon*

[3]*Laboratory of Mechanics, Department of Physics, Faculty of Science, University of Yaounde I, P.O. Box 812, Yaounde, Cameroon*

[4]*The Max Planck Institute for the Physics of Complex Systems Nöthnitzer Strasse 38, 01187 Dresden, Germany*

(Received 27 April 2014; revised manuscript received 25 July 2014; published 7 April 2015)

By using the F-expansion method associated with four auxiliary equations, i.e., the Bernoulli equation, the Riccati equation, the Lenard equation, and the hyperbolic equation, we present exact explicit solutions describing the dynamics of matter-wave condensates with time-varying two- and three-body nonlinearities. Condensates are trapped in a harmonic potential and they exchange atoms with the thermal cloud. These solutions include the generalized Jacobi elliptic function solutions, hyperbolic function solutions, and trigonometric function solutions. In addition, we have also found rational function solutions. Solutions constructed here have many free parameters that can be used to manipulate and control some important features of the condensate, such as the position, width, velocity, acceleration, and homogeneous phase. The stability of the solutions is confirmed by their long-time numerical behavior.

DOI: 10.1103/PhysRevE.91.042902 PACS number(s): 05.45.Yv, 03.75.Lm, 03.75.Kk, 34.20.Cf

I. INTRODUCTION

The dynamics of Bose-Einstein condensates (BECs) trapped in a harmonic potential and exchanging atoms with the thermal cloud has been a fascinating topic and has attracted much attention in recent theoretical and experimental works [1]. It is well known that the dynamical behavior of a condensate in the mean-field limit is well described by the Gross-Pitaevskii equation (GPE) [1], which is a nonlinear Schrödinger equation with an external potential. Basically, the GPE is a three-dimensional (3D) equation, but in some cases, it may be reduced to a one-dimensional (1D) form. This is possible when the condensate is frozen in two transverse directions by a stronger potential. The dimensionless governing equation of cigar-shaped (1D) BECs with two- and three-body nonlinearities can be written as [1]

$$\iota\Psi_t(x,t) + c\Psi_{xx} - g(t)|\Psi(x,t)|^2\Psi(x,t) - \chi(t)|\Psi(x,t)|^4\Psi(x,t) - (\alpha x^2 + \iota\gamma)\Psi(x,t) = 0. \quad (1)$$

In Eq. (1), the time t and the spatial coordinate x are scaled in the harmonic-oscillator units. The time-dependent cubic nonlinearity coefficient $g(t)$ characterizes the intensity of the two-body interactions. The quintic nonlinearity coefficient $\chi(t)$ characterizes the strength of the three-body interactions. Generally speaking, $\chi(t)$ is a complex quantity, but its imaginary part can be neglected since it is very small compared to the real part [2,3]. Thus, in the following, we consider that $\chi(t)$ is a real-valued expression. Time variations of the cubic and the quintic nonlinearities can be realized in condensates by magnetically or optically induced Feshbach resonances [1]. The parameter α represents the strength of the external magnetic or optical harmonic confinement. The complex quantity $\iota\gamma$, which is a nonconservative term, is introduced phenomenologically in Eq. (1). It takes into account the interaction between the condensate and the noncondensed fraction of the atomic vapor. When $\gamma > 0$, the density of the condensate grows due to an injection of atoms into the condensate from the thermal background or by a pumping mechanism from an atomic reservoir. For $\gamma < 0$, the density of the condensate decays since atoms are expelled out of the harmonic potential. This dissipative process can be explained by inelastic collisions in the BEC due to dipolar relaxation [1]. Hence, γ accounts for the exchange of atoms between the pure condensate and its surrounding thermal background. The rate of exchange of atoms is characterized by a temporal scale ζ, which is the time interval between subsequent events of adding or removing individual atoms from the atomic ensemble. The mean-field approximation GPE for BECs is applicable if ζ is negligible, i.e., $\zeta\omega_\perp \ll 1$, which is verified for typical configurations where $\omega_\perp = 2\pi \times 100$ Hz and $\zeta \sim 10$ μs [4]. In the absence of the three-body interactions $\chi(t) = 0$, Eq. (1) coincides with the cubic GPE with a gain or loss term (γ) employed in Refs. [5,6]. In Ref. [6], the cubic GPE with the gain term has been used to model the condensate growth in a trap, and it appears that as the condensate grows, its center of mass oscillates in the trap. In addition, the cubic GPE with the gain or loss term has been proposed to describe the dynamics of atom lasers [7], or light waves in fiber optics in the absence of harmonic confinement [8]. Some exact solutions of the cubic GPE with the gain or loss term γ have been reported [9]. In the case in which $\chi(t) = \gamma = 0$, Eq. (1) reduces to the well-known nonlinear Schrödinger equation. In such a case, there exists many kinds of exact solutions with the Hirota method, the inverse scattering method, the Darboux transformation, and the Lax pairs technique for describing bright-bright solitons, dark-dark solitons, bright-dark solitons, and so on in the existing literature.

Equation (1) (and its variant forms) is a nonlinear evolution equation, and it also appears in many fields in physics such as nonlinear optics, biophysics, fluids mechanics, and so on.

*Author to whom all correspondence should be addressed: belobodidier@gmail.com

It is rather difficult to solve Eq. (1) analytically, but in recent years many powerful and direct methods for finding exact solutions of Eq. (1) have emerged. Among them are the Bäcklund transformation [10], the tanh-function method [11], the extended tanh-function method [12], the homogeneous balance method [13], the auxiliary equation method [14], the F-expansion method [15], just to name a few. Exact solutions are of a relevant importance in physics in general, since as mathematical models they provide better understandings of physical models, and they may lead to physical applications. In the context of BECs, Mohamadou *et al.* [16] have recently derived exact solutions of Eq. (1) by using the extended-tanh function method with special solutions of an auxiliary equation, i.e., the Lenard equation. In addition, using the same method developed in Ref. [16], exact solutions of Eq. (1) with different geometrical traps have also been proposed by Wamba *et al.* [17] and Belobo *et al.* [18]. We recall that in Ref. [17], the trapping potential consists of a linear magnetic field and a time-dependent laser field, while in Ref. [18] the condensate is confined by a linear field and exchanges atoms with the thermal cloud. If we want to better understand the dynamical behavior of BECs trapped in a harmonic potential and exchanging atoms with the thermal cloud, a detailed investigation of Eq. (1) using more powerful methods to obtain more types of exact solutions containing soliton solutions is needed. Hence, using another method may lead to other solutions of Eq. (1).

The aim of this work is to construct exact solutions of Eq. (1) in the framework of the F-expansion method, combined with four types of auxiliary equations, i.e., the Bernoulli equation, the Riccati equation, the Lenard equation, and the hyperbolic equation.

The rest of the paper is organized as follows. In Sec. II, we present the model. Section III is devoted to deriving exact solutions of Eq. (1) by applying the F-expansion method, combining it with four types of auxiliary equations. We discuss some issues of our exact solutions in Sec. IV. Then, we show that it is possible to significantly increase the number of solutions obtained in Ref. [16] by using other solutions of the Lenard equation. Finally, Sec. V concludes the paper.

II. KINEMATICS OF THE CENTER OF MASS OF THE CONDENSATE

To derive exact solutions of Eq. (1), we need to transform Eq. (1) into a more tractable and manageable form. Toward that end, we follow Ref. [16] and use the following modified lens-type transformation:

$$\Psi(x,t) = D(t)\Phi(X,T)\exp[\eta(t) + \imath f(t)x^2], \tag{2}$$

where T is a function of time t, and $X = \frac{x}{l(t)}$. The function $f(t)$ represents the nonlinear frequency shift, and $\eta(t)$ (which takes into account the exchange of atoms between the condensate and its surroundings) represents the growth $[\eta(t) > 0]$ or the loss $[\eta(t) < 0]$ of atoms. The preservation of the scaling implies that $\frac{dT}{dt} = \frac{1}{l(t)^2}$. Further, we request that

$$\frac{df(t)}{dt} = -4cf(t)^2 - \alpha(t), \tag{3}$$

$$\frac{dD(t)}{dt} = -2cf(t)D(t), \tag{4}$$

$$\frac{dl(t)}{dt} = 4cf(t)l(t), \tag{5}$$

$$\frac{d\eta(t)}{dt} = \gamma. \tag{6}$$

Inserting Eq. (2) into Eq. (1) and using Eqs. (3)–(6) yields the reduced form of Eq. (1) in the rescaled variables X and T (see [16]),

$$\imath\frac{\partial\Phi(X,T)}{\partial T} = -c\frac{\partial^2\Phi(X,T)}{\partial X^2} - P^2|\Psi(X,T)|^2\Phi(X,T) + \chi_0|\Phi(X,T)|^4\Phi(X,T), \tag{7}$$

with $D(t) = [|g(t)|l(t)^2\exp[2\eta(t)]]^{-\frac{1}{2}}$, $\chi(t) = \chi_0 g(t)^2 l(t)^2$, $P^2 = -\mathrm{sgn}[g(t)]$. The two-body interactions are attractive if $P^2 = +1$, but they are repulsive when $P^2 = -1$. Equation (7) is a cubic-quintic GPE with constant parameters. The exact solution of Eq. (1) takes the form [16]

$$\Psi(x,t) = \sqrt{|G(t)|}\Phi(X,T) \times \exp\left\{\eta(t) + \imath\left[-\frac{1}{4c}\frac{d}{dt}\ln|G(t)|\right]x^2\right\}, \tag{8}$$

where $G(t) = g(t)\exp[2\eta(t)]$, $\eta(t) = \int_0^t \gamma dt' + \eta_0$, η_0 being a constant. Solution (8) is obtained by assuming that $l(t) = |G(t)|^{-1}$, $T(t) = \int_0^t G(t')^2 dt'$, $f(t) = \frac{1}{4c}\frac{d}{dt}\ln|G(t)|$.

Exact explicit solutions of Eq. (1) are obtained from the solution (8) if the explicit form of the function $\Phi(X,T)$ is given. To derive explicit expressions of $\Phi(X,T)$, we assume that it takes the amplitude-phase form and can be written as

$$\Phi(X,T) = Q(\xi)\exp[i\theta(X,T)], \tag{9}$$

where Q represents the amplitude part and θ accounts for the phase part. The variables ξ and θ have the forms

$$\xi = k_0X - \omega_0T, \quad \theta(X,T) = kX - \omega T. \tag{10}$$

Parameters k_0, k, ω_0, and ω are real constants that account for width, linear frequency shift, velocity, and the homogenous phase of the wave function $\Phi(X,T)$, respectively. Substituting Eqs. (9) and (10) into Eq. (7), and then separating the real and the imaginary parts, respectively, yields the following set of ordinary differential equations with respect to Q:

$$(\omega - ck^2)Q + Q^3 - \chi_0Q^5 + ck_0\frac{d^2Q}{d\xi^2} = 0, \tag{11}$$

$$(\omega_0 - 2ckk_0)\frac{d^2Q}{d\xi^2} = 0. \tag{12}$$

Assuming the constraint

$$\omega_0 = 2ckk_0 \tag{13}$$

means that we only need to solve Eq. (11). Thus, in the following, we focus our attention on deriving solutions of Eq. (11). We will assume that the function Q is expandable in a polynomial function $F(\xi)$, where F satisfies an

auxiliary equation. So far, there are some important physical properties that will be exhibited by the complete solutions to be constructed. For example, one may be interested in the dynamics of the center of mass of the condensate for a specific solution. The properties of the center of mass help us to understand the behavior of the condensate at mean. In the rescaled frame, the position, velocity, and acceleration of the condensate center of mass are $X_{\rm CM} = 2ckT$, $\dot{X}_{\rm CM} = 2ck$, and $\ddot{X}_{\rm CM} = 0$, respectively. In terms of the dimensionless physical variables, the position, velocity, and acceleration of the center of mass are $x_{\rm CM}(t) = (ck/\gamma)\sinh(2\gamma t)$, $\dot{x}_{\rm CM} = 2ck\cosh(2\gamma t)$, and $\ddot{x}_{\rm CM} = 4ck\gamma\sinh(2\gamma t)$, respectively. Hence, the behavior at mean of the condensate is affected by the rate of exchange of atoms between the condensate fraction and the uncondensed fraction, and by the linear frequency shift of the initial condition. These features, that are nowadays manageable in BEC experiments with a high accuracy, allow us to understand the influence that the interplay between the condensate and the uncondensed fraction has on the stability and the dynamics of the condensate. At initial time, the center of mass of the condensate is at the center of the trapping potential with the initial velocity $2ck$ without any acceleration. As time increases, the velocity and acceleration of the center of mass increase for negative and positive values of γ. This implies that the exchange of atoms with the thermal background accelerates the center of mass, such that the temperature of the core increases with time, and it may lead to the collapse of the condensate. However, for small values of γ, the acceleration and velocity of the core shall remain small such that the growth of the velocity induced by the atoms pumping, or the loss mechanisms, will be negligible, avoiding the collapse of the condensate. The linear frequency k may also be used to control the acceleration and the velocity of the condensate's core. In this work, one has two powerful tools to avoid the collapse of the condensate. The position of the center of mass as time evolves also depends on the sign of the linear frequency k, such that the condensate moves toward the left side to the axial potential if $k < 0$, while the condensate moves toward the right side of the potential for positive values of k. The features of the parameters γ and k may be used in some BEC applications such as the realization of the atomic laser where the velocity of atoms can be tuned by proper choices of the linear frequency and the rate of rate of exchange of atoms between the condensate and its surroundings. Another potential application is the transport of the condensate in experiments driven by the parameters γ and k. According to Newton's second law, the condensate can be considered as a classical particle moving in the effective potential $U_{\rm eff} = (-2ck/\gamma)\cosh(2\gamma t)$, with total energy $E = 2[ck\cosh(2\gamma t)]^2 - (2ck/\gamma)\cosh(2\gamma t)$, its only equilibrium point being located at the center of the trap, $x = 0$.

III. EXACT SOLUTIONS

A. The Bernoulli equation as an auxiliary equation

We suppose that the function Q has the following form:

$$Q(\xi) = \sum_{i=0}^{M} a_i F^i(\xi), \tag{14}$$

where M is a positive integer, a_i are real constants to be determined later, and the function F is the solution of the general Bernoulli equation,

$$\frac{dF}{d\xi} = aF(\xi) + bF^{\lambda}(\xi), \tag{15}$$

the parameters a, b, and λ being real constants that will be also determined later, with $\lambda \neq 1$. Introducing Eq. (14) into Eq. (11) and using the homogeneous balance between the highest-order derivative and nonlinear terms, respectively, yields $\lambda = 2M + 1$. Since $\lambda \neq 1$, then $M \geqslant 1$. Let us consider the simple case in which $M = 1$ and $\lambda = 3$. We have

$$Q(\xi) = a_0 + a_1 F(\xi), \qquad \frac{dF}{d\xi} = aF(\xi) + bF^3(\xi). \tag{16}$$

Inserting Eq. (16) into Eq. (11) and collecting coefficients of powers $F^i(\xi)$, then setting each coefficient to zero, yields a set of overdetermined algebraic equations for the unknowns a_0, a_1, a, b, and ω. Solving this set of overdetermined equations with the aid of MAPLE leads to the following solutions:

$$a_0 = 0, \tag{17}$$

$$a = \frac{-\sqrt{3}}{4k_0\sqrt{c}\sqrt{\chi_0}}, \tag{18}$$

$$b = \pm\frac{a_1^2\sqrt{\chi_0}}{k_0\sqrt{3c}}, \tag{19}$$

$$\omega = \frac{-3 + 16ck^2\chi_0}{16\chi_0}. \tag{20}$$

Equations (17) and (18) imply that $c > 0$ and $\chi_0 > 0$, meaning that solutions are valid only for repulsive three-body interactions. One infers from Eqs. (19) and (20) that the amplitude and the homogeneous phase of the wave function are sensitive to the strength of the three-body interaction $\chi(t)$. It is thus possible to tune to the desired values both the amplitude and the phase of the condensate externally by means of the Feshbach resonance technique. Inserting the solutions of the general Bernoulli equation [Eq. (15)] for $\lambda = 3$ [19] given in Appendix A into Eq. (16) leads to an explicit expression of Q. Hence, exact explicit solutions of Eq. (1) are

$$\begin{aligned}\Psi_{1j}(x,t) = {} & \sqrt{|G(t)|}a_1 F_{1j}(\xi)\exp[\imath\theta(X,T)] \\ & \times \exp\left\{\eta(t) + \imath\left[-\frac{1}{4c}\frac{d}{dt}\ln|G(t)|\right]x^2\right\}, \\ & j = 1,2,3.\end{aligned} \tag{21}$$

Equations (16)–(20) and the solutions of Appendix A imply that the heights of solutions (21) are proportional to the strength of the cubic nonlinearity, but inversely proportional to the strength of the quintic nonlinearity. Therefore, the experimenter knows how to manage the cubic and quintic nonlinearities in order to obtain a solution with an assumed amplitude. The density of a solution is subjected to a growth in the feeding regime, while the density decays when atoms are removed from the condensate. This feature has been predicted in Refs. [16,18]. In addition, the behavior of the density of the condensate is unchanged both for attractive and

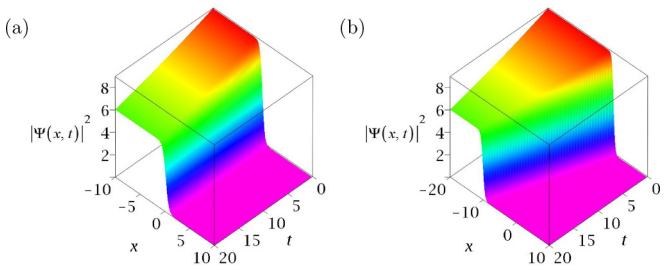

FIG. 1. (Color online) Spatiotemporal evolution of the wave function of Eq. (21) for $j = 2$. The parameters selected are $\alpha = -0.005$, $k_0 = 1$, $\chi_0 = \frac{1}{12}$, $a_1 = 1$, $c = 0.5$, $\eta_0 = 0$, $g(t) = -1$, and $\gamma = -0.005$. (a) $k = 0.01$, density profile of an antikink soliton with initial speed 0.01. (b) $k = -0.5$, effect of the linear frequency shift on the direction of the moving antikink soliton. The initial speed of the soliton is equal to $|k|$, and the direction of the soliton depends on the sign of k.

repulsive condensates. From (21), one understands that we have constructed three bunches of solutions of Eq. (1). To represent some samples of the solutions (21), we choose the following relevant physical parameters: $\alpha = -0.005$, $c = 0.5$, and $\eta(t) = \gamma t$ with $\eta_0 = 0$, used in some experimental and theoretical studies [16–21]. (We remind the reader that a slightly expulsive parabolic harmonic potential, negative value of α was used in the experiments of Refs. [20,21] to produce solitons in condensates.) We display in Fig. 1(a) the dynamics of the condensate's wave function, where we have set $j = 2$ in solution (21) with $\gamma = -0.005$, $\chi_0 = 1/12$, and $k = 0.01$. In this case, the solution (21) is an antikink soliton with initial velocity 0.01. The influence of the linear frequency shift on the direction of the condensate can be seen in Fig. 1(b), where $k = -0.5$. The moving antikink soliton evolves toward the left side of the cigar axis and its initial velocity amounts to 0.05. Kink and antikink solitons have been predicted in single condensates with two- and three-body nonlinearities in different trap geometries [16,17,18] and in binary condensates with cubic nonlinearities [22]. Other nonlinear media also allow the existence of kink and antikink solitons such as a layer of binary liquid heated from below, where oscillatory convection sets in via a subcritical bifurcation described by the cubic-quintic Ginsburg-Landau equation [23], optical fibers with elliptical birefringence for the evolution of the state of polarization of counterpropagating waves [24], the nonlinear dispersive fiber optics for the description of wave propagation by including the effects of group-velocity dispersion, self-phase-modulation, stimulated Raman scattering, and self-steepening [25]. The analytical expression of the antikink soliton solution found in Ref. [16] is different from the solution obtained in the present work by using the Bernoulli auxiliary equation. Moreover, with only fewer parameters, i.e., k and γ, we can characterize the behavior of the condensate at mean.

B. The Riccati equation as an auxiliary equation

We assume that the function Q takes the form

$$Q(\xi) = \sum_{i=-N}^{N} a_i F^i(\xi), \tag{22}$$

where the function F is the solution of the following Riccati equation [26]:

$$\frac{dF}{d\xi} = MF^{\lambda}(\xi) + \frac{\varepsilon}{1-\lambda} F^{2-\lambda}, \quad \varepsilon = \pm 1. \tag{23}$$

Inserting Eq. (22) into Eq. (11) and considering the homogeneous balance between the highest-order derivative and nonlinear terms, respectively, we obtain $\lambda = 2N + 1$. Let us now consider the simple case in which $N = 1$ and $\lambda = 3$. Equations (22) and (23) become

$$\begin{aligned} Q(\xi) &= a_0 + a_1 F(\xi) + a_2 F^{-1}(\xi), \\ \frac{dF}{d\xi} &= MF^3(\xi) - \frac{\varepsilon}{2} F(\xi). \end{aligned} \tag{24}$$

Introducing Eqs. (24) into Eq. (11), collecting coefficients of powers $F^i(\xi)$, and then setting each coefficient to zero, yields a set of overdetermined algebraic equations for the unknowns a_0, a_1, M, and ω. Solving these equations with the aid of MAPLE, we obtain

$$\begin{aligned} a_{11} &= \frac{1}{8c\sqrt{2k_0}} \left(\frac{3c}{\chi_0}\right)^{\frac{3}{4}}, \quad a_{21} = \sqrt{\frac{k_0}{2}} \left(\frac{3c}{\chi_0}\right)^{\frac{3}{4}}, \\ M_1 &= \frac{3}{128ck_0^2\chi_0}, \quad \omega_1 = ck^2 + \frac{3\varepsilon - 27}{128\chi_0}, \end{aligned} \tag{25}$$

$$a_{12} = -a_{11}, \quad a_{22} = -a_{21}, \quad M_1, \quad \omega_1, \tag{26}$$

$$a_{13} = -\imath a_{11}, \quad a_{23} = \imath a_{21}, \quad M_1, \quad \omega_1, \tag{27}$$

$$a_{14} = \imath a_{11}, \quad a_{24} = -\imath a_{21}, \quad M_1, \quad \omega_1, \tag{28}$$

$$a_{15} = a_{11}, \quad a_{25} = a_{21}, \quad -M_1, \quad \omega_2 = ck^2 - \frac{(3\varepsilon + 27)}{128\chi_0}, \tag{29}$$

$$a_{16} = -a_{11}, \quad a_{26} = -a_{21}, \quad -M_1, \quad \omega_2, \tag{30}$$

$$a_{17} = -\imath a_{11}, \quad a_{27} = \imath a_{21}, \quad -M_1, \quad \omega_2, \tag{31}$$

$$a_{18} = \imath a_{11}, \quad a_{28} = -\imath a_{21}, \quad -M_1, \quad \omega_2, \tag{32}$$

$$a_0 = 0. \tag{33}$$

Equation (28) implies that $c > 0$ and $\chi_0 > 0$ (the three-body interactions are repulsive). Using Eqs. (24)–(33), we derive exact solutions of Eq. (1),

$$\begin{aligned} \Psi_{2nm}(x,t) = \sqrt{|G(t)|}[a_{1n} F_{2m}(\xi) + a_{2n} F_{2m}^{-1}(\xi)] \exp[\imath\theta(X,T)] \\ \times \exp\left\{\eta(t) + \imath\left[-\frac{1}{4c}\frac{d}{dt}\ln|G(t)|\right]x^2\right\}, \end{aligned} \tag{34}$$

where n,m are integers, with $n = \overline{1,8}$, and $m = \overline{1,4}$ if $\varepsilon = -1$, $m = \overline{5,7}$ if $\varepsilon = +1$, and $m = 8$ if $\varepsilon = 0$. The solutions of the Riccati equation are given in Appendix B [26]. Equations (25)–(34) imply that the amplitudes of solutions (34) are highly dependent on the values of the width and the strength

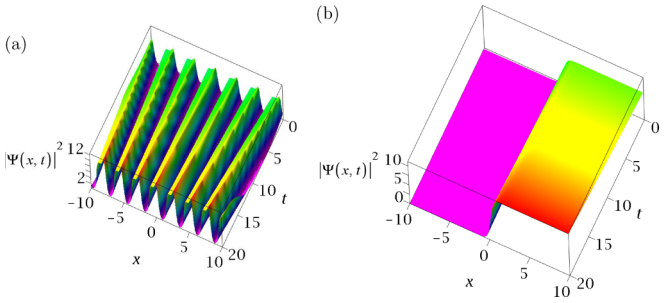

FIG. 2. (Color online) Propagation of the matter wave condensate of the solution given by Eq. (34). (a) Density profile of a growing periodic solution for $n = 5$, $m = 7$, and $\varepsilon = +1$. (b) Density profile of a moving kink soliton for $n = 5, m = 3$, and $\varepsilon = -1$. In both cases, the other parameters are the same as in Fig. 1(a), except $\chi_0 = 0.1$, $\gamma_0 = 0.005$.

of the quintic nonlinearity, which is also related to the atom feeding or loss parameter γ. The phases of solutions (34) are characterized by χ_0 and the free parameter k. Hence, after fixing the values of k_0, χ_0, and γ, it is possible to predict space-time evolution of the amplitude and the phase of solutions (34). Since the latter parameters can be precisely controlled externally in current BEC experiments, we infer that solutions (34) are likely to be observed in current or future experiments with condensates. We visualize in Figs. 2(a) and 2(b) the spatiotemporal evolutions of the wave function for two different cases of solution (34). In Fig. 2(a), we have set in Eq. (34) $n = 5$, $m = 7$, and $\varepsilon = 1$. We obtain a multiple bright soliton solution periodically spaced on the axial potential. The dynamical characteristics of the center of mass of this solution are the same as those of Fig. 1(a) since the same parameters were used. Multiple bright soliton solutions are usually obtained in condensates via the modulational instability. In the case of Eq. (1), multiple bright solitons were generated numerically in Ref. [27]. Here, we give an analytical expression of a multiple bright soliton solution in the framework of Eq. (1). Such moving periodic solutions may be observed in optical lattices, and they can be used to insert atoms onto optical devices, such as atom chips, waveguides, and mirrors [18,28]. Figure 2(b) portrays the spatiotemporal evolution of a kink soliton obtained for $n = 5$, $m = 3$, and $\varepsilon = -1$. This is a kink soliton solution of Eq. (1) that is different from that derived in Ref. [16].

C. The Lenard equation as an auxiliary equation

We search a function Q that has the form

$$Q(\xi) = \sum_{i=0}^{N} a_i F^i(\xi), \tag{35}$$

the function F satisfying the Lenard equation [29]

$$\frac{dF}{d\xi} = \sqrt{b_0 + b_2 F^2(\xi) + b_4 F^4(\xi) + b_6 F^6(\xi)}. \tag{36}$$

Solutions of (36) are given in Appendix C. Substituting Eq. (35) into Eq. (11) and considering the homogeneous balance between the highest-order derivative and nonlinear terms, respectively, we obtain $N = 1$. Inserting Q into Eq. (11), collecting coefficients of powers $F^i(\xi)$, and then equating each coefficient to zero, yields a set of overdetermined algebraic equations for the unknowns a_0, a_1, b_4, and ω. Solving them with MAPLE, we have

$$a_{11} = \sqrt{k_0}\left(\frac{cb_6}{\chi_0}\right)^{\frac{1}{4}}, \quad b_4 = -\frac{1}{2ck_0}\sqrt{\frac{2cb_6}{\chi_0}}, \tag{37}$$

$$a_{12} = -a_{11}, \quad b_4, \tag{38}$$

$$a_{13} = \imath a_{11}, \quad -b_4, \tag{39}$$

$$a_{14} = -\imath a_{11}, \quad b_4, \tag{40}$$

$$a_0 = 0, \quad \omega = ck^2 - ck_0^2 b_2. \tag{41}$$

Equation (37) implies that k_0 must be positive, and both χ_0 and b_6 must have the same sign. Inserting Eqs. (37)–(41) into Eq. (35) yields explicit solutions of Q, which in turn are used to obtain exact solutions of Eq. (1), which are

$$\Psi_{3nm}(x,t) = \sqrt{|G(t)|}a_{1n}F_{3,m}(\xi)\exp[\imath\theta(X,T)] \times \exp\left\{\eta(t) + \imath\left[-\frac{1}{4c}\frac{d}{dt}\ln|G(t)|\right]x^2\right\}, \tag{42}$$

where n,m are integers, with $n = \overline{1,4}$, and $m = \overline{1,18}$ for $b_0 = 0$ and $m = \overline{19,22}$ for $b_0 = \frac{8b_2^2}{27b_4}$ and $b_6 = \frac{b_4^2}{4b_2}$. Relations (37)–(40) mean that the amplitudes of solutions (42) depend on the values of k_0 and χ_0. Equation (41) implies that the phases of the solutions (42) depend on the values of k and k_0. After the choice of the parameters b_i ($i = 0,1,2,3,4,5,6$) related to the solution pattern needed, it is possible to precisely manipulate the amplitude and the phase of solutions only with the selection of the values of the width ($1/k_0$), the linear frequency k, the sign of χ_0, and the rate of exchange γ. There are many types of solutions of Eq. (1) that can be derived from Eq. (42). We present in Fig. 3(a) a bright soliton solution of (42) for $n = 1$, $m = 1$, with $b_2 = 2$, $b_6 = -2$, $\chi_0 = -0.1$, and $g(t) = 1$. The other parameters are the same as in Fig. 1(a). Bright solitons have been reported in condensate experiments with a constant two-body nonlinearity [20,21]. The dynamics of the core of this soliton are the same as that of the solution of Fig. 1(a). The parameter k_0 plays two important roles in the characterization of the solutions: (i) generally speaking, the width of the condensate is $1/k_0$; (ii) for each solution

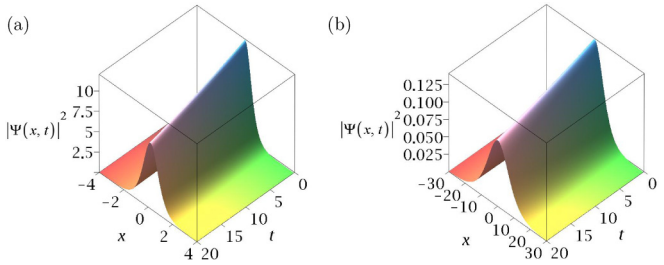

FIG. 3. (Color online) (a) Sample of a bright soliton solution derived from solution (42) for $n = 1, m = 1$ with $k_0 = 1$, $\chi_0 = -0.1$, $b_2 = 2$, and $b_6 = -2$. (b) Same parameters as in panel (a) except $k_0 = 0.1$. The parameter k_0 affects both the width and the amplitude of the solution. The other parameters as the same as in Fig. 1(a).

derived from Eq. (42), the amplitude is proportional to $\sqrt{k_0}$ as depicted by Eq. (37). A comparison between Figs. 3(a) and 3(b) corroborates the latter effects due to k_0.

One important class of physically relevant solutions of Eq. (1) is the Jacobi elliptic function solutions that are missed in the above development. We need to remedy this by including the generalized Jacobian elliptic solutions of Eq. (1). Toward that end, we resort the same procedure and consider the following special solutions of the Lenard equation [30–33], which can be found in Appendix D. The generalized Jacobi exact solutions of Eq. (1) can then be expressed as follows:

$$\Psi_{3nm}(x,t) = \sqrt{|G(t)|}a_{1n}F_{5,m}(\xi)\exp[\imath\theta(X,T)] \times \exp\left\{\eta(t) + \imath\left[-\frac{1}{4c}\frac{d}{dt}\ln|G(t)|\right]x^2\right\}, \quad (43)$$

where n,m are integers, with $n = \overline{1,4}$ and $m = \overline{18,19}$. These solutions have to respect the constraint imposed by the expression of b_4 given by Eq. (37), and they are valid only for negative values of χ_0. Thus, the generalized Jacobi function solutions (43) are valid provided that the quintic interatomic interactions are attractive, and they share the same features with solutions (42) regarding the behavior of the amplitudes and the phase. Subsequently, k_0 can be written in terms of the periods k_1 and k_2 as $k_0 = -\frac{1}{2cb4}\sqrt{\frac{2cb_6}{\chi_0}}$, with b_4 and b_6 chosen as in Eq. (37) or in Appendix D. In other words, once two periods k_1,k_2 are fixed, the width $1/k_0$ and the strength of the three-body interatomic interactions are derived. It is interesting to notice that, except for the atom feeding or loss mechanism that is controlled by γ, all important features of the solutions (43) depend on the values of the periods k_1,k_2. We plot in Fig. 4(a) the density profile of the generalized Jacobi cosine function, and in Fig. 4(b) the density profile of the generalized Jacobi function of the third kind, in the feeding regime $\gamma = 0.001$, for repulsive condensates $g = 1$. As periodic solutions, the generalized Jacobi elliptic function solutions may be observed for BECs in optical lattices [28]. Some particular solutions of (43), the Jacobi elliptic function solutions, have been reported in Jacobian elliptic potentials for condensates with constant cubic and cubic-quintic nonlinearities [34].

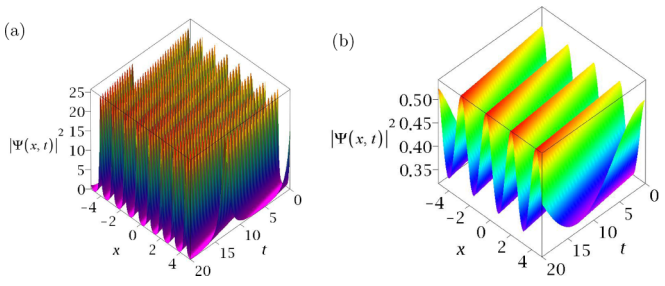

FIG. 4. (Color online) Spatiotemporal evolution of density profiles of generalized Jacobi elliptic solutions of Eq. (1). (a) $c(\xi,k_1,k_2)$, (b) $d_1(\xi,k_1,k_2)$. Parameters are $\alpha = -0.005$, $k_1 = 0.6$, $k_2 = 0.2$, $\chi_0 = -k_1^2k_2^2$, $\gamma = 0.001$, $k = 0.1$, and $g = 1$.

D. The hyperbolic equation as an auxiliary equation

The function Q is assumed to have the form

$$Q(\xi) = \sum_{i=0}^{N} a_i \sinh^i[F(\xi)], \quad (44)$$

where the function F satisfies the hyperbolic equation [35]

$$\frac{dF}{d\xi} = c_0 + c_2\sinh^2(\xi). \quad (45)$$

The solutions of the hyperbolic equation [35] are presented in Appendix E. Substituting Eq. (44) into Eq. (11) and considering the homogeneous balance between the highest-order derivative and nonlinear terms, respectively, we obtain $N = 1$. Then, introducing the function Q into Eq. (11), collecting all coefficients of powers $\sinh^i[F(\xi)]$, and setting each coefficient to zero yields a set of overdetermined algebraic equations for the unknowns a_0, a_1, c_0, and ω. Solving them with MAPLE, we obtain

$$a_{11} = \sqrt{k_0c_2\left(\frac{3c}{\chi_0}\right)^{\frac{1}{4}}},$$
$$\omega_1 = k_0c_2\sqrt{\frac{3c}{\chi_0}} + ck^2 + \frac{3ck_0^2c_2^2}{4} - \frac{3}{16\chi_0}, \quad (46)$$
$$c_{01} = \frac{-\sqrt{\frac{3c}{\chi_0}} - 2ck_0c_2}{4ck_0},$$

$$a_{12} = -a_{11}, \quad \omega_1, \quad c_{01}, \quad (47)$$

$$a_{13} = \imath a_{11}, \quad \omega_2 = -k_0c_2\sqrt{\frac{3c}{\chi_0}} + ck^2 + \frac{3ck_0^2c_2^2}{4} - \frac{3}{16\chi_0},$$
$$c_{02} = \frac{\sqrt{\frac{3c}{\chi_0}} - 2ck_0c_2}{4ck_0}, \quad (48)$$

$$a_{14} = -\imath a_{11}, \quad \omega_2, \quad c_{02}, \quad (49)$$

$$a_0 = 0. \quad (50)$$

Proceeding in a similar way as above, we obtain exact solutions of Eq. (1) as

$$\Psi_{4nm}(x,t) = \sqrt{|G(t)|}a_{1n}\sinh_{1,m}[F(\xi)]\exp[\imath\theta(X,T)] \times \exp\left\{\eta(t) + \imath\left[-\frac{1}{4c}\frac{d}{dt}\ln|G(t)|\right]x^2\right\}, \quad (51)$$

where $n,m = 1,2,3,4$. From Eqs. (46)–(50), one can realize that features of the solutions (51) are related to some experimental parameters such as the strength of the quintic interatomic interactions, the rate of exchange of atoms with the thermal background γ, and the linear frequency shift k. For instance, the amplitudes of solutions (51) depend on the width $(1/k_0)$ and the strength of the quintic interatomic interactions χ_0 (which depends on the interplay between the condensate and the thermal vapor), whereas the homogeneous phase depends on the width, linear phase, and χ_0. As already stated above, it is possible to control the amplitude and phase

of a solution in current condensate experiments once $1/k_0$, k, and γ have been fixed. In addition, the kinematics of the center of mass of the solutions (51) are also manageable externally in experiments, as mentioned before. We expect that the present work will motivate the quest of hyperbolic solutions in BEC experiments and applications.

E. Discussions

In the latter section, we have constructed exact solutions of Eq. (1) using a lens-type transformation with constraints [Eqs. (3)–(6)] also used in Ref. [16]. However, due to the method used in this work, the kinematics of the center of mass of our solutions is rather different from that predicted in Ref. [16]. In addition, we provide many types of solutions that are related to important experimental parameters with BECs. We have also proposed hyperbolic solutions and generalized Jacobi function solutions.

It is well known that the inclusion of quintic nonlinearity alters the behavior of matter-wave condensates. One important issue is to show what effects the quintic nonlinearity has on the formation of matter-wave condensates. To single out these effects, we consider the solutions with and without quintic nonlinearity for the four types of auxiliary equations. In the limit case of vanishing three-body interactions, the solutions found above actually have $\chi(t) = 0$ counterparts, since they exist for any arbitrary nonzero small values of $\chi(t)$, however their counterparts for $\chi(t) = 0$ cannot be expressed analytically simply due to divergence to infinity of some parameters [see Eqs. (18), (25), (37), and (46) for example]. Therefore, we resolve Eq. (1) again with $\chi(t) = 0$. For the case of the Bernoulli equation, the analytical solution is given by Eq. (21), where $a_1 F(\xi)$ is replaced by $a_0 + a_1 F(\xi)$, with $a_0 = \pm ck_0 a/\sqrt{-2c}$, $a_1 = \pm\sqrt{-2c}k_0 b$, and $\omega = \frac{1}{2}c(k_0^2 a^2 + 2k^2)$, a and b being free real parameters. The solutions exist only if the dispersion coefficient c is negative. Such solutions do not describe the evolution of matter-wave condensates, but they may rather describe the evolution of light waves in fiber optics with application to telecommunication transmissions. In addition, from Eq. (18) we know that the solutions with nonzero quintic nonlinearity are valid only for positive values of c. Due to the method adopted in the present work, the influence of quintic nonlinearity on the dynamics of waves cannot be determined because the solutions obtained describe two distinct physical situations (positive

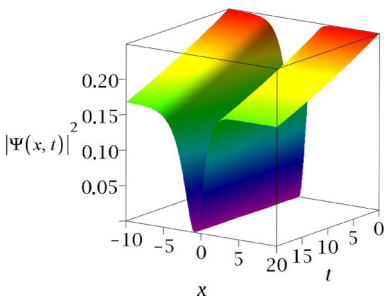

FIG. 5. (Color online) Evolution of the density of a dark soliton of Eq. (1) obtained using the Bernoulli equation, with the same parameters as in Fig. 1(a) except $c = -0.5$, $a = 1$, $b = -1$, and $\chi(t) = 0$.

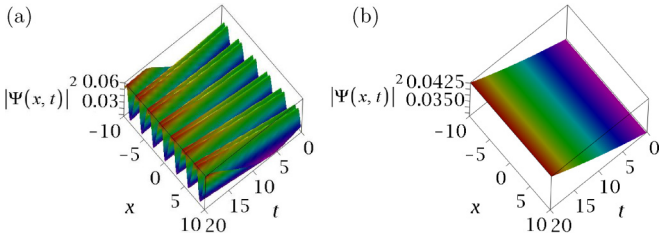

FIG. 6. (Color online) (a) Evolution of the density of a periodic solution of Eq. (1) obtained using the Riccati equation, with same parameters as in Fig. 2(a) except $M = -0.4$, $\chi(t) = 0$. (b) Evolution of the density of a plane-wave solution of Eq. (1) derived using the Riccati equation, with the same parameters as in Fig. 2(b), except $M = -0.4$, $\chi(t) = 0$.

dispersion coefficient $c > 0$ and negative dispersion coefficient $c < 0$). A comparison between Fig. 5 [$\chi(t) = 0$] and Fig. 1(a) confirms that with the inclusion of quintic nonlinearity, the dynamics of waves are different with regard to the shape of the solution, which turns from a dark profile to an antikink profile. When one uses the Riccati equation, the solution of Eq. (1) is given by Eq. (34), where $n = \overline{1,5}$; m and ε have the same signification. The coefficients are $a_{11} = 0$, $a_{21} = \sqrt{-2c}\varepsilon k_0$, $\omega_1 = ck^2 + 2ck_0^2 M\varepsilon$; $a_{12} = 0$, $a_{22} = -a_{11}$, $\omega_2 = \omega_1$; $a_{13} = -2ck_0^2 M^2$, $a_{23} = 0$, $\omega_3 = \omega_1$; $a_{14} = a_{13}$, $a_{24} = a_{21}, \omega_4 = 6ck_0^3 M^2\sqrt{-2c}\varepsilon + ck^2 + 2ck_0^2 M\varepsilon$; $a_{15} = a_{13}, a_{25} = -a_{24}$, $\omega_5 = -6ck_0^3 M^2\sqrt{-2c}\varepsilon + ck^2 + 2ck_0^2 M\varepsilon$. M is a free real parameter. The expressions of the coefficients a_{1i} and a_{2i} show that only the coefficients for $n = 3$ correspond to matter-wave solutions. The others with a negative dispersion coefficient may rather describe the evolution of light in fiber optics. A comparison between Fig. 6(a) [$\chi(t) = 0$] and Fig. 2(a) implies that the inclusion of quintic nonlinearity modifies the top of the periodic solution. In addition, drawing a parallel between Fig. 6(b) and Fig. 2(b), one realizes that the inclusion of quintic nonlinearity may also induce the localization of matter waves in BECs. Localized solutions are due to a compensation between dispersion and nonlinearity. It is likely that the quintic nonlinearity helps to attain a regime of parameters where the nonlinearities balance the dispersion. Resolving Eq. (1) for $\chi(t) = 0$ with the hyperbolic equation, the solutions are provided by Eq. (51) for the parameters $a_1 = a_2 = 0$ and $\omega = -a_0^2 + ck^2$, where a_0 is a free parameter. Once again, due to the reason mentioned above, quintic nonlinearity also induces the localization of solutions since the cubic form

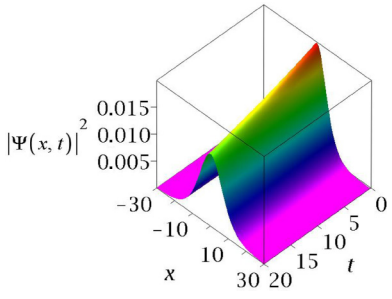

FIG. 7. (Color online) Evolution of the density of a bright solution of Eq. (1) obtained using the ordinary auxiliary equation, with the same parameters as in Fig. 2(a) except $M = -0.4$, $\chi(t) = 0$.

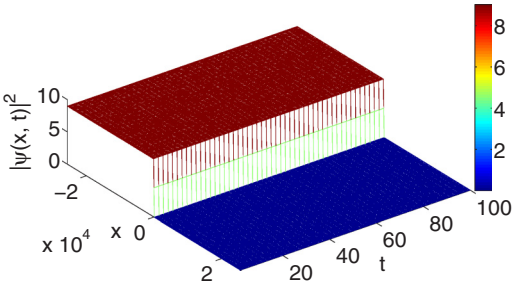

FIG. 8. (Color online) Spatiotemporal propagation of the stable antikink-like soliton of Fig. 1(a). Parameters are the same as in Fig. 1(a) except $\gamma = 0$.

of Eq. (1) only admits plane-wave solutions (due to the fact that $a_1 = a_2 = 0$.) Setting $\chi(t) = 0$ in Eq. (1), the Lenard equation reduces to the ordinary auxiliary equation since one must set $b_6 = 0$ [12]. In this case, it is difficult to check the impact the quintic nonlinearity has on the formation of matter-wave condensates because the ordinary auxiliary equation has different solutions, which are presented in Appendix F [23]. The solutions of the cubic equation found by means of the ordinary auxiliary equation are given by Eq. (43), where $n = 1,2$, with $a_1 = \pm\sqrt{-2cb_4}k_0$ and $\omega = ck^2 - ck_0^2 b_2$. The solutions found may describe the evolution of matter-wave condensates provided that $c > 0$, which implies that $b_4 < 0$. The inclusion of the quintic nonlinearity does not bring significant changes, as can be seen by comparing Figs. 7, 3(a), and 3(b).

IV. NUMERICAL SIMULATIONS

An important issue concerning exact solutions found with mathematical methods is their stability or robustness in real physical experiments. The physical relevance of an exact solution can be investigated by means of comparisons with the exact numerical solution obtained by a direct integration of the underlying Eq. (1). Here, the numerical method used is the split-step Fourier method [36,37]. The spatial grid is sufficiently large in order to prevent problems with the boundaries [37]. An initial reasonably small amount of random perturbation is added in order to unveil any instability that can be seeded during the time evolution. We restrict ourselves to some of the cases of exact solutions found above.

Let us start with the antikink soliton solution of (21) for $j = 2$. In the case in which $\gamma = 0$, the condensate does not exchange any atoms with a thermal background. Figure 8 proves that the initial condition persists without destruction though the insertion of a small initial random perturbation. For a condensate in the regime of a loss of atoms, there is also very good agreement between the analytical prediction and numerical results, as depicted by Figs. 9(a)–9(c), for $\gamma = -0.005$. Figure 9(d) shows that the disturbed initial condition remains stable during the propagation. One can then consider that such a solution is a robust physical object that can be observed in a real experiment.

Next, we look at the kinklike soliton solution of Fig. 2(b). Two cases are considered, namely the feeding regime and the regime where the condensate does not exchange any atom with its surroundings. In Fig. 10(a) ($\gamma = 0$), the amplitude of the condensate stays constant during the propagation, while the amplitude increases with time in the feeding regime, as shown in Figs. 10(b)–10(d) ($\gamma = 0.005$). From Figs. 10(a) and 10(e) ($\gamma = 0.005$), one infers that the derived kinklike soliton solution of (37) for $n = 5$, $m = 3$, and $\varepsilon = -1$ is a stable solution.

The bright soliton solution of Fig. 3(b) obtained by using the Lenard equation is dynamically stable and accurately corroborates its analytical counterpart. Figure 11 displays the agreement between the numerical and analytical solutions,

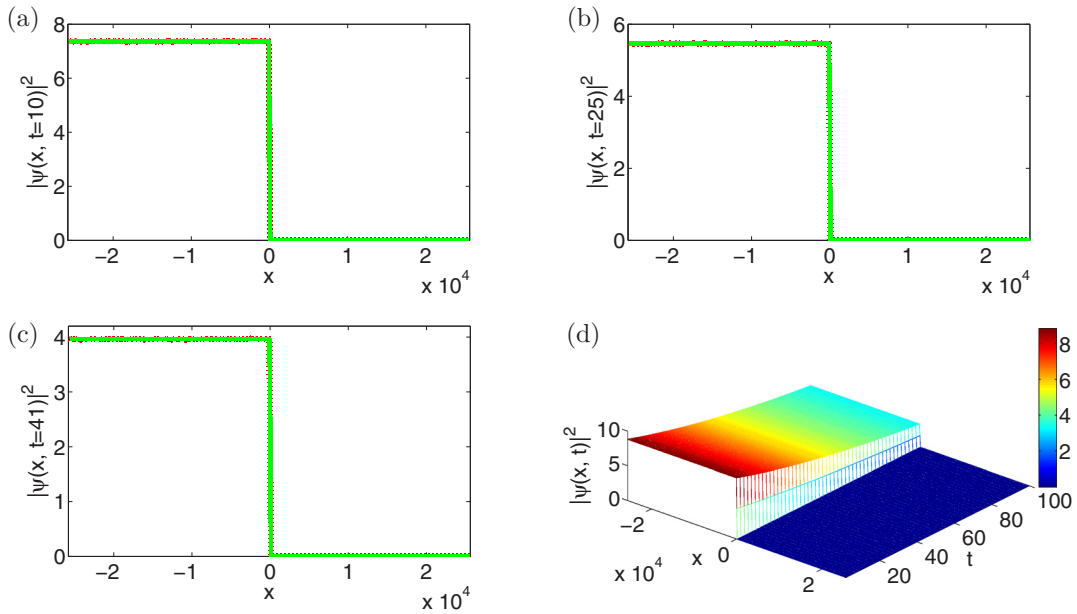

FIG. 9. (Color online) (a)–(c) Comparison between analytical (solid line) and numerical (dotted line) solutions at particular times of the antikink-like soliton of Fig. 1(a). (d) Spatiotemporal evolution of the stable antikink-like soliton of Fig. 1(a). Parameters are the same as in Fig. 1(a).

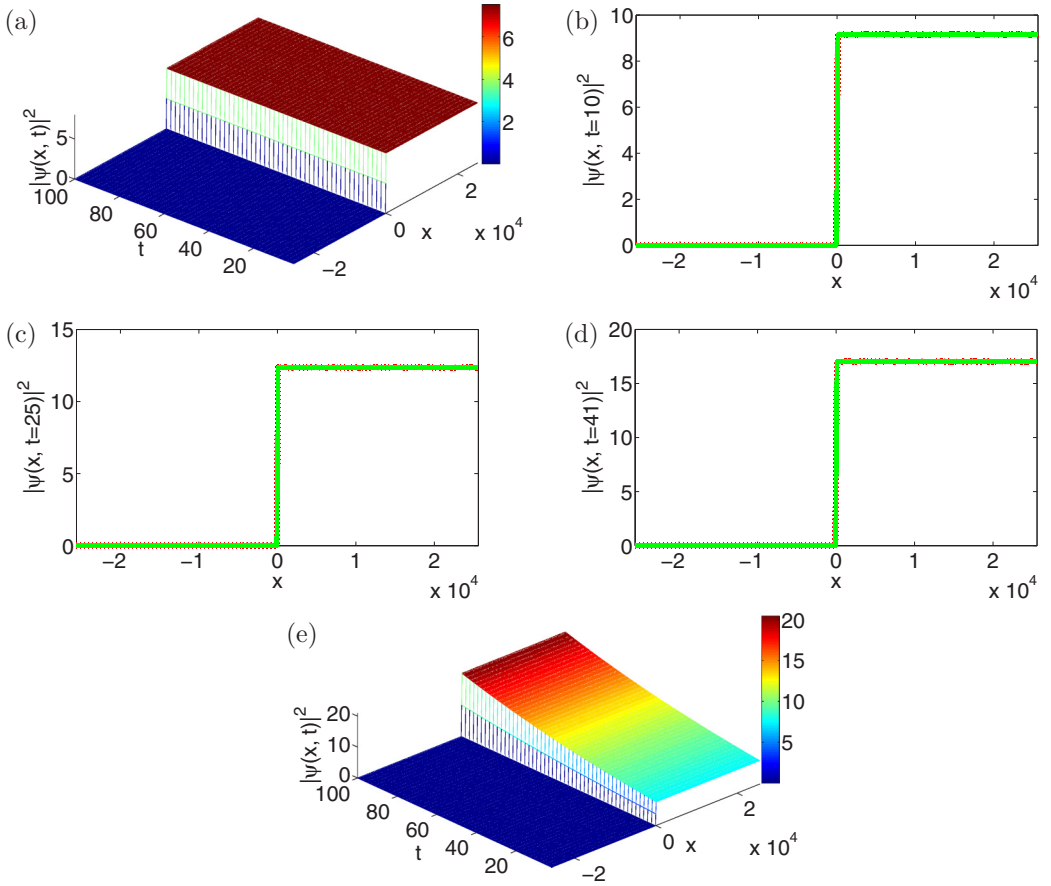

FIG. 10. (Color online) (a)–(c) Parallel between analytical (solid line) and numerical (dotted line) solutions at different times of the kinklike soliton of Fig. 2(b). (d) Spatiotemporal propagation of the stable antikink-like soliton. Parameters are the same as in Fig. 2(a).

as well as the long-time robustness of our bright soliton [Fig. 3(a)].

In the above discussions, we have shown that an analytical solution for the case $\chi = 0$ and $c > 0$ is not available for the physical situation of matter waves in condensates if one uses the Bernoulli equation as an auxiliary equation. To show how far the qualitative behavior changes, we display in Fig. 12 the spatiotemporal evolution of the condensate density with

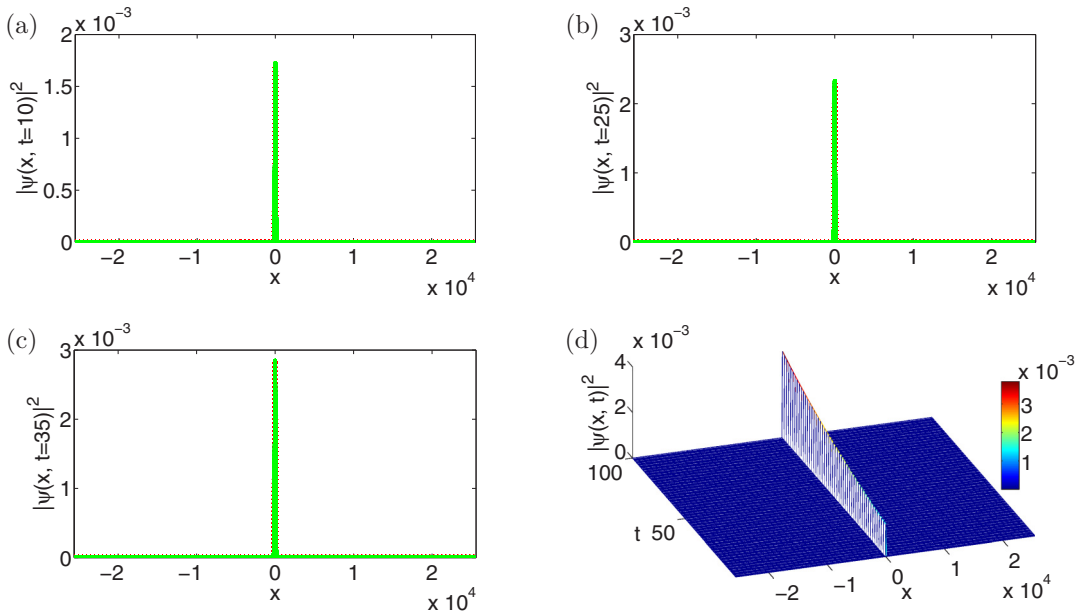

FIG. 11. (Color online) (a)–(c) Parallel between analytical (solid line) and numerical (dotted line) solutions at different times of the bright soliton of Fig. 3(b). (d) Spatiotemporal propagation of the stable bright soliton. Parameters are the same as in Fig. 3(b) except $\gamma = 0.005$.

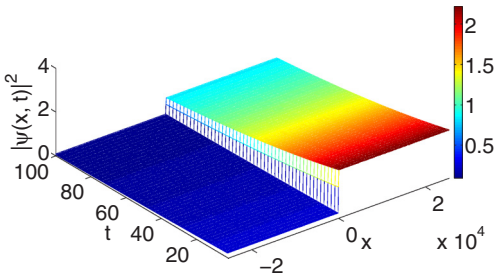

FIG. 12. (Color online) Spatiotemporal evolution of a stable kink solution for $\chi = 0$, $c = 0.5$. The solution is that of Fig. 5 with the same parameters except that of c.

the same parameters as in Fig. 5, except $c = 0.5$. As one can see, we obtain a stable kink profile solution, the maximum density of which is 2.21. The analytical solution with $c > 0$ for a (vanishingly) small value of χ is an antikink solution with very large density, confirming the previous analysis.

The dynamical stability of some trivial-phase dark, kink, and antikink soliton solutions of Eq. (1) has been analyzed mathematically and numerically in Ref. [10]. Here, the dynamical stability of more valuable nontrivial phase solutions is investigated numerically. The stability of the specific solutions that were tested is well verified. Families of solutions constructed here may also be applied in other physical media where Eq. (1) also appears, such as nonlinear fiber optics.

V. CONCLUSION

In this paper, we have studied the GPE with time-dependent two- and three-body nonlinearities, confined in a harmonic potential and exchanging atoms with the thermal background. By applying the F-expansion method, and taking advantage of solutions of four types of auxiliary equations, i.e., the Bernoulli equation, the Riccati equation, the Lenard equation, and the hyperbolic equation, we have constructed 230 explicit exact solutions of Eq. (1), distributed into 49 families. Among these solutions, we have hyperbolic function solutions and trigonometric functions solutions. Furthermore, we have also found rational function solutions. In comparison with the work done in Ref. [10], we have found more exact solutions of Eq. (1) and we analyzed the stability of some nontrivial phase soliton solutions numerically. The latter nontrivial phase solitons appear to be dynamically stable. The effects of quintic nonlinearity on the formation of matter-wave condensates are also studied in certain cases. It appears that the inclusion of quintic nonlinearity drastically modifies the shape of solutions found with the Riccati and hyperbolic auxiliary equations, and it could lead to localization of solutions. This localization can come from the fact that the inclusion of quintic nonlinearity alters the nonlinearities in such a way that they compensate the dispersion.

When the parameter γ is not small, Eq. (1) formally describes the evolution of condensates at finite temperatures where the effects of the thermal cloud become important. Many models have been developed in order to account for the effects of the thermal cloud [38]. Indeed, through a recent self-consistent investigation of the whole thermal cloud part (i.e., the noncondensed and the anomalous densities) by means of a variational time-dependent Hartree-Fock-Bogoliubov theory, the impact of the anomalous density in three- and two-dimensional homogeneous Bose gases at finite temperatures has been analyzed [39,40]. The parameter γ can be related to the so-called Keldysh self-energy [41,42]. Comparisons between some finite-temperature BEC models have been performed in Ref. [42]. The dynamics of dark solitons within a finite-temperature BEC model with only two-body interatomic interactions has been reported in Ref. [43]. Nevertheless, many finite-temperature BEC models rarely consider the effects of three-body interactions. For instance, a study of the effects of finite temperature (γ large) on the dynamics of solitons in matter waves of BECs with two- and three-body interatomic interactions should be carried out in future works.

ACKNOWLEDGMENTS

D.B.B. acknowledges the hospitality of the Abdus Salam International Center for Theoretical Physics (Trieste, Italy), where a part of this work was done. D.B.B. is indebted to B. Deconinck and R. Carretero-González for useful discussions on the numerics. T.C.K. is grateful for the hospitality of the Max-Planck Institute for the Physics of Complex Systems in Dresden. The authors acknowledge anonymous reviewers for useful comments and suggestions.

APPENDIX A: SOLUTIONS OF THE GENERAL BERNOULLI EQUATION

The solutions of the general Bernoulli equation according to Ref. [13] are found to be as follows:

$$F_{11}(\xi) = \left(-\frac{a}{2b}\right)^{\frac{1}{2}}; \tag{A1}$$

$$\xi_0 > 0: F_{12}(\xi) = -\frac{a}{2b}\left[\tanh\left(a\xi - \frac{\ln(\xi_0)}{2}\right) + 1\right]^{\frac{1}{2}}; \tag{A2}$$

$$\xi_0 < 0: F_{13}(\xi) = -\frac{a}{2b}\left[\coth\left(a\xi - \frac{\ln(-\xi_0)}{2}\right) + 1\right]^{\frac{1}{2}}. \tag{A3}$$

APPENDIX B: SOLUTIONS OF THE RICATTI EQUATION

The solutions of the general Bernoulli equation according to Ref. [20] are found to be as follows:

$$F_{21}(\xi) = \left\{\sqrt{\frac{-1}{M(\lambda-1)}}\tanh[\sqrt{-M(\lambda-1)}\xi]\right\}^{\frac{1}{\lambda-1}}; \tag{B1}$$

$$F_{22}(\xi)=\left\{\sqrt{\frac{-1}{M(\lambda-1)}}\coth[\sqrt{-M(\lambda-1)}\xi]\right\}^{\frac{1}{\lambda-1}}; \tag{B2}$$

$$F_{23}(\xi)=\left(\sqrt{\frac{-1}{M(\lambda-1)}}\left\{\sqrt{\frac{-1}{M(\lambda-1)}}\tanh[\sqrt{-M(\lambda-1)}\xi]\pm\iota\,\mathrm{sech}[\sqrt{-M(\lambda-1)}\xi]\right\}\right)^{\frac{1}{\lambda-1}}; \tag{B3}$$

$$F_{24}=\left\{\sqrt{\frac{-1}{M(\lambda-1)}}\left[\frac{\sqrt{2}\sqrt{\frac{-1}{M(\lambda-1)}}\tanh[\sqrt{-M(\lambda-1)}\xi]\pm\iota\,\mathrm{sech}[\sqrt{-M(\lambda-1)}\xi]}{\sqrt{2}-\mathrm{sech}[\sqrt{-M(\lambda-1)}\xi]}\right]\right\}^{\frac{1}{\lambda-1}}; \tag{B4}$$

$$F_{25}(\xi)=\left\{-\sqrt{\frac{-1}{M(\lambda-1)}}\tan[\sqrt{-M(\lambda-1)}\xi]\right\}^{\frac{1}{\lambda-1}}; \tag{B5}$$

$$F_{26}(\xi)=\left\{\sqrt{\frac{-1}{M(\lambda-1)}}\cot[\sqrt{-M(\lambda-1)}\xi]\right\}^{\frac{1}{\lambda-1}}; \tag{B6}$$

$$F_{27}=\left\{-\sqrt{\frac{-1}{M(\lambda-1)}}\left[\frac{\sqrt{2}\sqrt{\frac{-1}{M(\lambda-1)}}\tan[\sqrt{-M(\lambda-1)}\xi]\pm\iota\,\sec[\sqrt{-M(\lambda-1)}\xi]}{\sqrt{2}+\sqrt{5}\sec[\sqrt{-M(\lambda-1)}\xi]}\right]\right\}^{\frac{1}{\lambda-1}}; \tag{B7}$$

$$F_{28}=\left\{\frac{1}{-M(\lambda-1)\xi+p}\right\}^{\frac{1}{\lambda-1}}. \tag{B8}$$

p is an arbitrary real constant.

APPENDIX C: SOLUTIONS OF THE LENARD EQUATION

The Lenard equation admits the following solutions [23]:

$$b_2>0,\quad b_4<0,\quad b_6<0,\quad \delta=b_4^2-4b_2b_6>0{:}F_{3,1}=\sqrt{\frac{2b_2\mathrm{sech}^2(\sqrt{b_2}\xi)}{2\sqrt{\delta}-(\sqrt{\delta}+b_4)\mathrm{sech}^2(\sqrt{b_2}\xi)}},$$

$$F_{3,2}=\sqrt{\frac{2b_2\mathrm{csch}^2(\pm\sqrt{b_2}\xi)}{2\sqrt{\delta}+(\sqrt{\delta}-b_4)\mathrm{csch}^2(\pm\sqrt{b_2}\xi)}}; \tag{C1}$$

$$b_0=0,\quad b_2<0,\quad b_4\geqslant 0,\quad b_6<0,\delta>0{:}F_{3,3}=\sqrt{\frac{-2b_2\sec^2(\sqrt{-b_2}\xi)}{2\sqrt{\delta}-(\sqrt{\delta}-b_4)\sec^2(\sqrt{-b_2}\xi)}},$$

$$F3{,}4=\sqrt{\frac{2b_2\csc^2(\pm\sqrt{-b_2}\xi)}{2\sqrt{\delta}+(\sqrt{\delta}+b_4)\csc^2(\pm\sqrt{-b_2}\xi)}}; \tag{C2}$$

$$b_6=\frac{b_4^2}{4b_2},\quad b_2>0,\quad b_4<0{:}F_{3,5}=\sqrt{\frac{-b_2}{b_4}}[1+\tanh(\pm\sqrt{b_2}\xi)],\quad F_{3,6}=\sqrt{\frac{-b_2}{b_4}}[1+\coth(\sqrt{b_2}\xi)]; \tag{C3}$$

$$b_2>0{:}F_{3,7}=\sqrt{\frac{-b_2b_4\mathrm{sech}^2(\sqrt{b_2}\xi)}{b_4^2-b_2b_6[1+\tanh^2(\sqrt{b_2}\xi)]}},\quad F_{3,8}=\sqrt{\frac{b_2b_4\mathrm{csch}^2(\sqrt{b_2}\xi)}{b_4^2-b_2b_6[1+\coth^2(\sqrt{b_2}\xi)]}},$$

$$F_{3,9}=4\sqrt{\frac{b_2\exp(2\sqrt{b_2}\xi)}{\exp(4\sqrt{b_2}\xi-4C_4)-64b_2b_6}}; \tag{C4}$$

$$b_2>0{:}F_{3,7}=4\sqrt{\frac{b_2\exp(2\sqrt{b_2}\xi)}{\exp[(2\sqrt{b_2}\xi-4C_4)^2-64b_2b_6]}};\quad b_2>0,\quad \delta>0{:}F_{3,10}=\sqrt{\frac{2b_2}{\sqrt{\delta}\cosh(2\sqrt{b_2}\xi)-b_4}}; \tag{C5}$$

$$b_2>0,\quad \delta<0{:}F_{3,11}=2\sqrt{\frac{2b_2}{\sqrt{-\delta}\sinh(2\sqrt{b_2}\xi)-b_4}}; \tag{C6}$$

$$b_2 < 0, \quad \delta > 0: F_{3,12} = \sqrt{\frac{2b_2}{\sqrt{\delta}\sin(2\sqrt{-b_2}\xi) - b_4}}, \quad F_{3,13} = \sqrt{\frac{2b_2}{\sqrt{\delta}\cos(2\sqrt{-b_2}\xi) - b_4}}; \tag{C7}$$

$$b_2 > 0, \quad b_6 > 0; \quad F_{3,14} = \sqrt{\frac{-b_2\mathrm{sech}^2(\sqrt{b_2}\xi)}{b_4 + 2\sqrt{b_2 b_6}\tanh(\sqrt{b_2}\xi)}}, \quad F_{3,15} = \sqrt{\frac{b_2\mathrm{csch}^2(\sqrt{b_2}\xi)}{b_4 + 2\sqrt{b_2 b_6}\coth(\sqrt{b_2}\xi)}}; \tag{C8}$$

$$b_2 < 0, \quad b_6 > 0: F_{3,16} = \sqrt{\frac{-b_2\sec^2(\sqrt{-b_2}\xi)}{b_4 + 2\sqrt{-b_2 b_6}\tan(\sqrt{-b_2}\xi)}}, \quad F_{3,17} = \sqrt{\frac{-b_2\csc^2(\sqrt{-b_2}\xi)}{b_4 + 2\sqrt{-b_2 b_6}\cot(\sqrt{-b_2}\xi)}}; \tag{C9}$$

$$b_2 > 0, \quad b_4 = 0: F_{18} = 4\sqrt{\frac{\pm b_2\exp(2\sqrt{b_2}\xi)}{1 - 64 b_2 b_6\exp(4\sqrt{b_2}\xi)}}; \tag{C10}$$

$$b_2 < 0, \quad b_4 > 0: F_{3,19} = \sqrt{\frac{-8b_2\tanh^2\left(\pm\sqrt{\frac{-b_2}{3}}\xi\right)}{3b_4[3 + \tanh^2\left(\pm\sqrt{\frac{-b_2}{3}}\xi\right)]}}, \quad F_{3,20} = \sqrt{\frac{-8b_2\coth^2\left(\pm\sqrt{\frac{-b_2}{3}}\xi\right)}{3b_4[3 + \coth^2\left(\pm\sqrt{\frac{-b_2}{3}}\xi\right)]}}; \tag{C11}$$

$$b_2 > 0, \quad b_4 < 0: F_{3,21} = \sqrt{\frac{8b_2\tan^2\left(\pm\sqrt{\frac{b_2}{3}}\xi\right)}{3b_4[3 - \tan^2\left(\pm\sqrt{\frac{b_2}{3}}\xi\right)]}}, \quad F_{3,22} = \sqrt{\frac{8b_2\cot^2\left(\pm\sqrt{\frac{b_2}{3}}\xi\right)}{3b_4[3 - \cot^2\left(\pm\sqrt{\frac{b_2}{3}}\xi\right)]}}. \tag{C12}$$

$b_0 = 0$ corresponds to $F_{3,1} - F_{3,18}$; $b_0 = \frac{8b_2^2}{27b_4}$ and $b_6 = \frac{b_4^2}{4b_2}$ correspond to $F_{3,19} - F_{3,22}$.

APPENDIX D: GENERALIZED JACOBI ELLIPTIC FUNCTION SOLUTIONS OF THE LENARD EQUATION

Some generalized Jacobi elliptic function solutions of the Lenard equation [25–27] are as follows:

$$b_0 = 1 - k_1^2 - k_2^2 + k_1^2k_2^2, \quad b_2 = -1 + 2k_1^2 + 2k_2^2 - 3k_1^2k_2^2, \quad b_4 = -k_1^2 - k_2^2 + 3k_1^2k_2^2, \quad b_6 = -k_1^2k_2^2: F_{23} = c(\xi,k_1,k_2); \tag{D1}$$

$$b_0 = -1 + k_1^2 - k_2^2 + k_1^{-2}k_2^2, \quad b_2 = 2 - k_1^2 + 2k_2^2 - 3k_1^{-2}k_2^2, \quad b_4 = -1 - k_2^2 + 3k_1^{-2}k_2^2, \quad b_6 = -k_1^{-2}k_2^2: F_{24} = d_1(\xi,k_1,k_2). \tag{D2}$$

$c(\xi,k_1,k_2)$ is the generalized Jacobi elliptic cosine function, and $d_1(\xi,k_1,k_2)$ is the generalized Jacobi elliptic function of the third kind. The generalized Jacobi elliptic functions can be written in terms of the standard Jacobi elliptic functions as follows: $c(\xi,k_1,k_2) = k_3 cn(k_3\xi,k_4)/\sqrt{1 - k_2^2cn^2(k_3\xi,k_4)}$, $d_1(\xi,k_1,k_2) = \sqrt{k_1^2 - k_2^2}dn(k_3\xi,k_4)/\sqrt{k_1^2 - k_2^2dn^2(k_3\xi,k_4)}$, with $k_3 = \sqrt{1 - k_2^2}$, $k_4 = \sqrt{(k_1^2 - k_2^2)/(1 - k_2^2)}$, $0 \leqslant k_2 \leqslant k_1 \leqslant 1$. The generalized Jacobi functions degenerate to traditional functions in some limiting cases. For instance, if $k_2 \to 0$, one can obtain the usual Jacobi elliptic function solutions: $c(\xi,k_1,0) \to cn(\xi,k_1)$, $d_1(\xi,k_1,0) \to dn(\xi,k_1)$. If $k_1 \to 1, k_2 \to 0$, one obtains hyperbolic solutions: $c(\xi,1,0), d(\xi,1,0) \to \mathrm{sech}(\xi)$. For $k_1 \to 0, k_2 \to 0$, the generalized Jacobi elliptic functions degenerate to trigonometric solutions: $c(\xi,0,0) \to \cos(\xi)$, $d_1(\xi,0,0) \to 1$.

APPENDIX E: SOLUTIONS OF THE HYPERBOLIC EQUATION

Some solutions of the hyperbolic equation [29]:

$$c_2 > 0, \quad c_0c_2 - c_2^2 > 0, \quad c_2 - 2c_0 + 2\sqrt{c_0(c_2 - c_0)}\tan\{\sqrt{[c_0(c_2 - c_0)]}\xi\} > 0:$$

$$\sinh_{11}[F(\xi)] = \left\{\frac{(c_0 - \sqrt{c_0(c_2 - c_0)}\tan\{\sqrt{[c_0(c_2 - c_0)]}\xi\})^2}{c_2(c_2 - 2c_0 + 2\sqrt{c_0(c_2 - c_0)}\tan\{\sqrt{[c_0(c_2 - c_0)]}\xi\})}\right\}^{\frac{1}{2}}; \tag{E1}$$

$$c_2 > 0, \quad c_0c_2 - c_2^2 < 0, \quad c_2 - 2c_0 + 2\sqrt{c_0(c_2 - c_0)}\cot\{\sqrt{[c_0(c_2 - c_0)]}\xi\} > 0:$$

$$\sinh_{12}[F(\xi)] = \left\{\frac{(c_0 - \sqrt{c_0(c_2 - c_0)}\cot\{\sqrt{[c_0(c_2 - c_0)]}\xi\})^2}{c_2(c_2 - 2c_0 + 2\sqrt{c_0(c_2 - c_0)}\cot\{\sqrt{[c_0(c_2 - c_0)]}\xi\})}\right\}^{\frac{1}{2}}; \tag{E2}$$

$$c_2 > 0, \quad c_0c_2 - c_0^2 < 0, \quad c_2 - 2c_0 - 2\sqrt{c_0(c_2-c_0)}\coth\{\sqrt{-[c_0(c_2-c_0)]}\xi\} > 0:$$
$$\sinh_{13}[F(\xi)] = \left\{\frac{(c_0 + \sqrt{-c_0(c_2-c_0)}\coth\{\sqrt{-[c_0(c_2-c_0)]}\xi\})^2}{c_2(c_2-2c_0-2\sqrt{-c_0(c_2-c_0)}\coth\{\sqrt{-[c_0(c_2-c_0)]}\xi\})}\right\}^{\frac{1}{2}}; \tag{E3}$$

$$c_2 < 0, \quad c_0c_2 - c_0^2 < 0, \quad c_2 - 2c_0 - 2\sqrt{c_0(c_2-c_0)}\tanh\{\sqrt{-[c_0(c_2-c_0)]}\xi\} < 0:$$
$$\sinh_{13}[F(\xi)] = \left\{\frac{(c_0 + \sqrt{-c_0(c_2-c_0)}\tanh\{\sqrt{-[c_0(c_2-c_0)]}\xi\})^2}{c_2(c_2-2c_0-2\sqrt{-c_0(c_2-c_0)}\tanh\{\sqrt{-[c_0(c_2-c_0)]}\xi\})}\right\}^{\frac{1}{2}}. \tag{E4}$$

APPENDIX F: SOLUTIONS OF THE ORDINARY AUXILIARY EQUATION

The auxiliary equation admits the following solutions [23]:

$$b_0 = \kappa^2 - 1, \quad b_2 = 2 - \kappa^2, \quad b_4 = -1{:}F_{3,1} = dn(\xi); \tag{F1}$$
$$b_0 = 1 - \kappa^2, \quad b_2 = 2\kappa^2 - 1, \quad b_4 = -\kappa^2{:}F_{3,2} = cn(\xi); \tag{F2}$$
$$b_0 = -1, \quad b_2 = 2 - \kappa^2, \quad b_4 = \kappa^2 - 1{:}F_{3,3} = 1/dn(\xi); \tag{F3}$$
$$b_0 = 1, \quad b_2 = 2\kappa^2 - 1, \quad b_4 = \kappa^2(-1+\kappa^2){:}F_{3,4} = sn(\xi)/dn(\xi); \tag{F4}$$
$$b_0 = -2\kappa^3 + \kappa^4 + \kappa^2, \quad b_2 = 6\kappa - \kappa^2 - 1, \quad b_4 = -4/\kappa{:}F_{3,5} = \kappa dn(\xi)cn(\xi)/[1+\kappa sn^2(\xi)]; \tag{F5}$$
$$b_0 = 2 - 2\kappa_1 - \kappa^2, \quad b_2 = -6\kappa_1 - \kappa^2 + 2, \quad b_4 = -4\kappa_1{:}F_{3,6} = \kappa^2 sn(\xi)cn(\xi)/[\kappa_1 + dn^2(\xi)]; \tag{F6}$$
$$b_0 = (\kappa^2-1)/4\left(D_3^2\kappa^2 - D_2^2\right), \quad b_2 = (\kappa^2+1)/2, \quad b_4 = \left(D_3^2\kappa^2 - D_2^2\right)(\kappa^2-1)/4:$$
$$F_{3,7} = \sqrt{\left(D_2^2 - D_3^2\right)/\left(D_2^2 - D_3^2\kappa^2\right)}sn(\xi); \tag{F7}$$
$$b_0 = (2\kappa - \kappa^2 - 1)/D_2^2, \quad b_2 = 2\kappa^2 + 2, \quad b_4 = -D_2^2\kappa^2 - D_2^2 - 2D_2^2\kappa^2{:}F_{3,8} = [\kappa^2 sn^2(\xi) - 1]/D_2[\kappa sn^2(\xi) + 1]; \tag{F8}$$
$$b_0 = -(2\kappa + \kappa^2 + 1)/D_2^2, \quad b_2 = 2\kappa^2 + 2, \quad b_4 = -D_2^2(\kappa^2 + 1 + 2\kappa){:}F_{3,9} = [\kappa sn^2(\xi) + 1]/D_2[\kappa sn^2(\xi) - 1]; \tag{F9}$$
$$b_0 = b_4 = (\kappa^2-1)/4, \quad b_2 = (\kappa^2+1)/2{:}F_{3,10} = dn(\xi)/[1 \pm \kappa sn(\xi)], \quad F_{3,11} = \kappa sd(\xi) \pm nd(\xi); \tag{F10}$$
$$b_0 = -(1-\kappa^2)/4, \quad b_2 = (\kappa^2+1)/2, \quad b_4 = -1/4{:}F_{3,12} = \kappa sd(\xi) \pm nd(\xi); \tag{F11}$$
$$b_0 = 0, \quad b_2 > 0, \quad b_4 < 0{:}F_{3,13} = \sqrt{-b_2/b_4}\,\mathrm{sech}(\sqrt{b_2}\xi); \tag{F12}$$

where κ $(0 < \kappa < 1)$ denotes the modulus of the Jacobi elliptic function, $\kappa_1 = \sqrt{1-\kappa^2}$, and D_2, D_3 $(D_2D_3 \neq 0)$, and D_4 are arbitrary constants.

[1] *Emergent Nonlinear Phenomena in Bose-Einstein Condensates. Theory and Experiment*, edited by P. G. Kevrekidis, D. J. Frantzeskakis, and R. Carretero-González (Springer-Verlag, Berlin, 2008), and references therein.

[2] C. P. Search, W. Zhang, and P. Meystre, Phys. Rev. Lett. **92**, 140401 (2004).

[3] K. M. R. van der Stam, R. Meppelink, J. M. Vogels, and P. van der Straten, Phys. Rev. A **75**, 031602 (2007).

[4] V. A. Brazhnyi, V. V. Konotop, V. M. Pérez-García, and H. Ott, Phys. Rev. Lett. **102**, 144101 (2009).

[5] C. Yuce and A. Kilic, Phys. Rev. A **74**, 033609 (2006); L. Wu, R-J. Jiang, Y. H. Pei, and J-F. Zhang, *ibid.* **75**, 037601 (2007).

[6] P. D. Drummond and K. V. Kheruntsyan, Phys. Rev. A **63**, 013605 (2000).

[7] B. Kneer, T. Wong, K. Vogel, W. P. Schleich, and D. F. Walls, Phys. Rev. A **58**, 4841 (1998); A. M. Guzman, M. Moore, and P. Meystre, *ibid.* **53**, 977 (1996).

[8] R. Atre, P. K. Panigrahi, and G. S. Agarwal, Phys. Rev. E **73**, 056611 (2006); V. N. Serkin and A. Hasegawa, Phys. Rev. Lett. **85**, 4502 (2000); V. I. Kruglov, A. C. Peacock, and J. D. Harvey, *ibid.* **90**, 113902 (2003).

[9] L.-C. Zhao, Z.-Y. Yang, T. Zhang, and K.-J. Shi, Chin. Phys. Lett. **26**, 120301 (2009).

[10] *Bäcklund and Darboux Transformations*, edited by A. Coely *et al.* (American Mathematical Society, Providence, RI, 2001), and references therein.

[11] H. A. Abdusalam, Int. J. Nonlin. Sci. Numer. Simul. **6**, 99 (2005).

[12] Z. Y. Yan, Phys. Lett. A **292**, 100 (2001).

[13] M. L. Wang, Phys. Lett. A **213**, 279 (1996).

[14] E. Yomba, Chaos Solitons Fractals **21**, 75 (2004).

[15] Y. B. Zhou, M. L. Wang, and Y. M. Wang, Phys. Lett. A **308**, 31 (2003).

[16] A. Mohamadou, E. Wamba, D. Lissouck, and T. C. Kofane, Phys. Rev. E **85**, 046605 (2012).

[17] E. Wamba, T. C. Kofane, and A. Mohamadou, Chin. Phys. B **21**, 070504 (2012).
[18] D. Belobo Belobo, G. H. Ben-Bolie, and T. C. Kofane, Phys. Rev. E **89**, 042913 (2014).
[19] W. X. Ma and B. Fuchssteiner, Int. J. Nonlin. Mech. **31**, 329 (1996).
[20] L. Khaykovich, F. Schreck, G. Ferrari, T. Bourdel, J. Cubizolles, L. D. Carr, Y. Castin, and C. Salomon, Science **296**, 1290 (2002).
[21] K. E. Strecker, G. B. Partridge, A. G. Truscott, and R. G. Hulet, New J. Phys. **5**, 73 (2003).
[22] N. Dror, B. A. Malomed, and J. Zeng, Phys. Rev. E **84**, 046602 (2011).
[23] W. van Saarloos and P. C. Hohenberg, Phys. Rev. Lett. **64**, 749 (1990); V. Hakim, P. Jacobsen, and Y. Pomeau, Europhys. Lett. **11**, 19 (1990); B. A. Malomed and A. A. Nepomnyashchy, Phys. Rev. A **42**, 6009 (1990).
[24] S. Wabnitz, PIERS ONLINE **5**, 621 (2009).
[25] G. P. Agrawal and C. Headley III, Phys. Rev. A **46**, 1573 (1992).
[26] S. Zhang, Y. N. Sun, J. M. Ba, and L. Dong, J. Adv. Math. Studies **3**, 125 (2010).
[27] A. Mohamadou, E. Wamba, S. Y. Doka, T. B. Ekogo, and T. C. Kofane, Phys. Rev. A **84**, 023602 (2011).
[28] O. Morsch and M. Oberthaler, Rev. Mod. Phys. **78**, 179 (2006); G. K. Campbell, Ph.D. thesis, MIT, 2006.
[29] L-H. Zhang, Appl. Math. Comput. **208**, 144 (2009).
[30] E. A-B. Abdel-Salam, Z. Naturforsch. a **64**, 639 (2009).
[31] H. F. Baker, *Abelian Functions* (Cambridge University Press, Cambridge, 1897).
[32] P. F. Byrd and M. D. Friedman, *Handbook of Elliptic Integrals for Engineers and Physicists* (Springer, Berlin, 1954).
[33] E. T. Whittaker and G. N. Watson, *A Course of Modern Analysis. An Introduction to the General Theory of Infinite Processes and of Analytic Functions* (Cambridge University Press, Cambridge, 1996).
[34] J. C. Bronski, L. D. Carr, B. Deconinck, and J. N. Kutz, Phys. Rev. Lett. **86**, 1402 (2001); J. C. Bronski, L. D. Carr, B. Deconinck, J. N. Kutz, and K. Promislow, Phys. Rev. E **63**, 036612 (2001); B. Deconinck, B. A. Frigyik, and J. N. Kutz, Phys. Lett. A **283**, 177 (2001).
[35] S. D. Zhu, Chaos Solitons Fractals **34**, 1608 (2007).
[36] D. Belobo Belobo, G. H. Ben-Bolie, T. B. Ekogo, and T. C. Kofane, Int. J. Theor. Phys. **52**, 1415 (2013).
[37] G. P. Agrawal, *Nonlinear Fiber Optics* (Academic, San Diego, 2006), and references therein.
[38] N. P. Proukakis and B. Jackson, J. Phys. B **41**, 203002 (2008), and references therein.
[39] A. Boudjemâa and M. Benarous, Phys. Rev. A **84**, 043633 (2011).
[40] A. Boudjemâa, Phys. Rev. A **86**, 043608 (2012).
[41] H. T. C. Stoof, J. Low Temp. Phys. **114**, 11 (1999).
[42] S. P. Cockburn, A. Negretti, N. P. Proukakis, and C. Henkel, Phys. Rev. A **83**, 043619 (2011).
[43] S. P. Cockburn, H. E. Nistazakis, T. P. Horikis, P. G. Kevrekidis, N. P. Proukakis, and D. J. Frantzeskakis, Phys. Rev. Lett. **104**, 174101 (2010).